

Eksploatacja i Niezawodnosc - Maintenance and Reliability

Volume 29 (2027), Issue 3

https://ein.org.pl

The Polish Maintenance Society

PoC for a system to monitor overloads on the chassis of a high-mobility wheeled vehicle

Mariusz Kosobudzki[1,*]

[1] Katedra Podstaw Konstrukcji Maszyn i Układów Mechatronicznych, Politechnika Wrocławska, Poland
* Corresponding Author: mariusz.kosobudzki@pwr.edu.pl

Received: 23 April 2026
Revised: 2 October 2026
Accepted: 13 November 2026
Online: 20 November 2026

This is an open access article under the CC BY 4.0 license

Abstract

High-mobility wheeled vehicles are usually constructed by joining a base chassis with a specialized body. During the vehicle's service life, the loads on its load-bearing structure may, in certain situations, approach or even exceed admissible values and cause even permanent deformation, eliminating the vehicle from further use. Such loads may arise not only whilst driving (primarily in off-road and cross-country conditions), but also when additional equipment installed on the vehicle chassis is used incorrectly. An example of such a situation would be when a container structure joined to a chassis with an additionally armored cab is lifted to a position in which the vehicle's wheels do not touch the ground. In this case, the load-bearing structure between the cab and the container is subjected to bending, but in the opposite direction to that which occurs whilst driving. Such loads can lead to significant stress and strain on key load-bearing components of the vehicle and, for safety reasons, should be monitored. The load history of the vehicle's structural components can be determined by designing an appropriate measurement system. This article presents a PoC (Proof of Concept) for a system to monitor overloads in the load-bearing structure of a high-mobility off-road vehicle, based on an original transducer designed especially for this purpose to measure the deformation of the vehicle frame side member, adapted to work with a system for the acquisition and processing of measurement data.

Keywords: *maintenance system, high-mobility wheeled vehicle, health usage and monitoring system, transducer*

Article citation:
Kosobudzki M, PoC for a system to monitor overloads on the chassis of a high-mobility wheeled vehicle, Eksploatacja i Niezawodnosc – Maintenance and Reliability 2027: 29(3) http://doi.org/10.17531/ein/242866

Highlights

- PoC of an on-line system for monitoring overloads of the vehicle load-bearing structure.
- Design of an original transducer to measure the load of the load-bearing structure.
- Global transformation in the maintenance system of special and specialized high-mobility wheeled vehicles.

1. Introduction

High-mobility off-road vehicles are designed to operate in a variety of road conditions (on-road) [1,2] as well as in off-road and cross-country terrain [3]. They are the primary means of transport for the military. Such vehicles have a complex design and are equipped with specialized equipment, which results in high maintenance costs [4]. To design and manufacture a reliable and cost-effective high-mobility vehicle, it is necessary to acquire the appropriate experience and necessary data, such as knowledge of operational load spectra. Only then can a vehicle be produced that meets the required specifications [5]. In the case of military vehicles, additional, difficult-to-meet requirements emerge: the vehicles are to be dedicated to performing specific tasks (need to increase the number of vehicle variants), whilst at the same time their operation should be simple, standardized and ensure high levels of technical readiness (need to limit the number of vehicle variants). The starting point for achieving a compromise is to accept the concept that a specialized vehicle is to be built by joining a universal chassis [e.g. 4x4, 6x6, 8x8] and a special-purpose body, whilst the maintenance system will be based on carrying out pre-defined servicing tasks using technical diagnostics [6,7].

However, there is constant pressure to improve vehicle technical readiness rates. This has a direct impact on operational

readiness, which in turn drives changes to the current maintenance and training systems. In the world's largest armies, efforts are being made to move away from pre-scheduled maintenance tasks towards a reliability-centred maintenance (RCM) system [8]. The RCM is also normalized [9]. A significant challenge in introducing a new, effective maintenance system is access to reliable data describing the technical condition of the vehicle (and its components) and its change in correlation with operating conditions and service history. Establishing such correlations would allow for the monitoring of the progressive deterioration of the vehicle (and its components) in real time and the determination of the optimal time to carry out preventive maintenance activities. [10]. Such a continuous analysis, based on data collected from a network of sensors connected to a central processing unit (CPU), is performed by Health Usage and Monitoring Systems (HUMS), the first implementation of which was on a Chinook military helicopter [11]. Since then, aircraft and helicopters have been equipped with such systems. Unfortunately, there are currently no off-the-shelf industrial HUMS solutions for wheeled vehicles. This is due to a number of reasons, including finding a correlation between the measurable signal representing the load profile and the progressive degradation of the component under consideration, the balance between the number of load profile measurement points (the number of sensors) and the accuracy of the load profile recording (the type of sensors), and finally the complexity of the algorithm processing the measurement data and the required computational capabilities (online or offline analysis). Systems for monitoring the technical condition of vehicle assemblies and components require constant access to reliable data. Hence, there is a visible trend towards the development of new sensors, their integration into measurement and analysis modules, and the universalization of these modules for the entire range of vehicles from a given manufacturer. In the case of special-purpose vehicles, their small production scale and specific requirements mean that standard electronic systems for motor vehicles cannot be easily applied here. To monitor the required vehicle load conditions, it is often necessary to design an original transducer that converts the observed physical phenomenon into an easily identifiable measurement signal [12].

In order to identify the desired correlations between changes in the technical condition of the assembly and the load profile, and to determine the limit states, it is necessary to carry out appropriate tests. Such long-term vehicle tests for the U.S. Army are conducted, for example, at the Aberdeen Test Center [13]. The course of the tests and the correlations found between the vehicle's operating conditions and the values of selected loads are presented in [12]. In 2021, GPMS, together with AM General and the U.S. Army, conducted a demonstration of the capabilities of the HUMS Foresight MX system, dedicated to HUMVEE vehicles [14]. This system was originally developed for aircraft. The U.S. Army recently reported that the use of a HUMS demonstrator on the Abrams tank improves its operational readiness [15]. In Germany, similar research is being carried out, amongst others, at the Bundeswehr Technical Centre for Land-Based Vehicle Systems, Engineer and General Field Equipment (WTD 41) [16]. For the French Army, such research was carried out by the DGA Techniques terrestres centre in Angers [17]. In 2020, a dedicated HUMS system was implemented in 20 VAB vehicles, which was assessed positively following six months of testing [18]. In the case of the British Army, vehicle testing are being taken place, for example, at UTAC Millbrook [19]. The performance of HUMS systems for General Dynamics' PIRANHA Mk5 8x8 vehicles [20] and BAE Systems' PANTHER CLV [21] was assessed positively. These vehicles are currently in service. In Poland, military vehicle tests are being carried out by the Military Institute of Armoured and Automotive Technology in Sulejówek [22]. At research centres, vehicles are tested according to specific usage scenarios described in military standards [23], and on this foundation, a correlation is established between wear and tear and operating conditions.

Two main approaches are used to determine limit states: one based on the analytical or experimental determination of a component's fatigue life, followed by continuous monitoring of the load history (primarily for components subjected to fatigue loads) (model-based methods); and the other based on condition assessment (data-driven methods). In the case of high-mobility vehicles, multi-component structural systems, such as the load-bearing structure, suspension or powertrain components, are particularly difficult to monitor. A general problem concerning the determination of the correlation

between the load history and the limit state in relation to a vehicle can be found, for example, in [24]. In article [25], the authors presented the influence of the driver's driving style (from mild to aggressive) on the scope of necessary vehicle repairs by indicating the MTBF value. Article [26] presents a method for determining the load history of a vehicle frame for the purpose of estimating its durability using measurement signals from acceleration sensors. Another group of authors [27] presented an analysis of the influence of spring leaf manufacturing technology on their fatigue life. The analysis also covered stabilisers. In articles [28,29], the authors analysed the compliance of the FEM model of a leaf spring with experimental data, which directly contributes to the acceleration of determining the limit values of the spring's durability. The influence of the transfer case on load profiles in a complex drivetrain system of heavy high-mobility vehicles is presented in [30]. An example of research investigating the relationship between the technical condition of the tested unit (engine) and measurement data is presented in [12,31]. The authors constructed a measurement system consisting of 80 channels connected via a J1939 CAN bus. Sensors installed in the vehicle and additional sensors added for the purposes of the research were utilized. In summary, they concluded that they were able to predict the critical condition of an engine with a 10–15-minute warning by analyzing changes in the level and temperature of fluids in the lubrication and cooling systems. Similar research was conducted by the Australian Army [32]. Based on the examples presented, it can be concluded that the use of COTS sensors is limited when it comes to monitoring load profiles or assessing the technical condition of selected systems and components of high-mobility vehicles. This is most often due to the fastening system of these sensors and the quality of the measurement signals. In other words, dedicated sensors installed in appropriate locations on the vehicle are often required to monitor selected loads. An example of a dedicated measurement system for monitoring structural overloads in a universal high-mobility wheeled vehicle is presented in this article. A key component of this system is a dedicated, specially designed transducer for measuring the deformation of the vehicle frame side member.

In summary, at the chosen level of development of the suggested solutions (PoC), the approach to addressing the problem of monitoring high-mobility wheeled vehicle load-bearing structure overloads under selected operating conditions was presented in the following steps: the operational concept of the monitoring system was established; an analysis of the distribution of loads and displacements of the load-bearing structure components under the assumed operating conditions was performed; suitable and accessible locations for mounting the measuring transducer were identified; the range of deformations to be measured by the transducer was calculated; an original transducer body was designed and equipped with an appropriate sensing system; the deformation threshold triggering the recording of such an event was determined; and a system for recording overloads of the vehicle's load-bearing structure was designed. The proposed solutions are discussed in the individual chapters. It should be noted that the proposed solution is not described in the available literature.

2. Material and methods

An example of a baseline chassis that serves as a universal wheeled platform of high mobility is the Jelcz 8x8 vehicle, a version of which is shown in Figure 1. This platform is preliminarily prepared, among other things, for container installation, connection to a self-loading hook system, specialized weaponry, flatbed or a telecommunications mast from the MMC mobile communication node, which can be extended to a height of more than 30 m [33].



Figure 1. Jelcz P882D.43 universal chassis adapted for connection with specialized bodies, e.g. flatbed, container, hook self-loading system [34].

The design of the base chassis considered basic (constant and variable) and exceptional loads (which could be predicted at the design stage) resulting from the use of various types of

special equipment. An example of exceptional loads occurring in the version of the chassis with an additionally armored cab was the use of equipment installed on a container platform, which required the entire vehicle to be lifted and levelled to operate. It can be said that this particular case of vehicle use was associated with the highest risk of overloading the load-bearing structure. In this position, the vehicle's wheels did not touch the ground. Under such conditions, the vehicle's load-bearing structure between the cab and the specialized bodies was subjected to bending, but in the opposite direction to that which occurs during driving. The resulting deflection of the frame side members was so significant that, for safety reasons, the load had to be monitored. Both this case and other possible vertical loads resulting from the specific conditions of operation of the body equipment and driving have an impact on vehicle deterioration and should be monitored in modern maintenance systems.

As a result of the analysis of possible exceptional loads on the load-bearing structure of a universal wheeled platform, a concept for a monitoring system to record overloads was developed, which could consist of two basic components: a transducer to measure the longitudinal deformation (bending) of the frame (no COTS sensor suitable for this application was found) and an electronic system to acquire and process measurement data. Initially, it was assumed that the monitoring system should operate independently of other vehicle control and measurement systems. The following basic functions of the system were adopted: tracking overloads of the longitudinal members of the load-bearing structure in the vertical longitudinal plane (e.g. during lifting and lowering of the container) with data recording: date, time, number of exceedances of the allowable load value, maximum load value, possibility of setting a permissible load threshold value, recording on an SD memory card (minimum 1000 events), communication via RJ45 interface, power supply from the vehicle's on-board network, system prepared for CAN communication.

3. Results

The development of the transducer concept involved the following main stages: establishing the operating conditions for the transducer, designing the transducer base so that it could be easily installed on an existing vehicle in a suitable location and designing the strain gauge arrangement, including transducer calibration and zeroing of the initial indication.

3.1. Boundary conditions for transducer operation

Preliminary data for the analysis of the stress and strain distribution in the load-bearing structure were taken under selected operating conditions of the entire vehicle and the location of the transducer installation [35]. The boundary conditions for the operation of the transducer were determined by referring to the strength data of the members of the vehicle side and their geometry. The cross-sectional dimensions of the side members in the analyzed section are shown in Figure 2. The material used to manufacture these elements is S500MC steel.

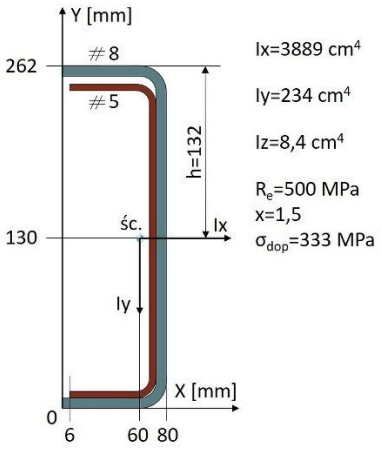


Figure 2. Cross-section of the longitudinal side member of the frame, its selected geometric dimensions, and material data.

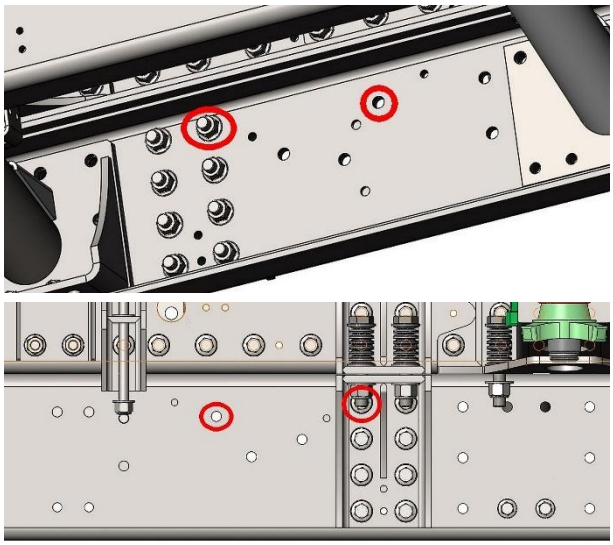


Figure 3. Layout of existing holes and indication of transducer mounting points.

After inspecting the vehicle, the preliminary location for

installing the transducer was selected. At the indicated locations for transducer installation, the longitudinal member had a cross-section of the C shape reinforced with an additional C-shaped profile, as shown in Figures 2 and 3.

It was initially assumed that no additional mounting holes would be made - the installation would be carried out using the existing ones. The layout of the selected transducer mounting holes is shown in Figures 3 and 4. The distance between the indicated mounting holes was l=230 mm.

Assuming that the longitudinal member will be subjected to maximum permissible bending, the elongation Δl_x of points spaced at a distance of $l_x = 230$ mm on the upper flange of the longitudinal member will be:

$$\varepsilon = \frac{\Delta l_x}{l_x} = \frac{\sigma_{dop}}{E} \rightarrow \Delta l_x = \frac{\sigma_{dop} \cdot l_x}{E} = \frac{333 \cdot 230}{2{,}1 \cdot 10^5} = 0{,}365\ mm = 365\ \mu m \quad (1)$$

where: σ_{dop} – permissible stress (333 MPa), E - Young's modulus for steel (2,1x10^5 MPa).

Due to the real location of the transducer mounting, as shown in Figure 4, there will be less elongation between its mounting points (compared to the upper flange of the longitudinal member):

$$\Delta l = \frac{\Delta l_x \cdot cos\alpha \cdot (h - \frac{a+b}{2})}{h} = \frac{0{,}365 \cdot 0{,}995 \cdot (132 - \frac{43+66}{2})}{132} = 0{,}211\ mm = 211\ \mu m \quad (2)$$

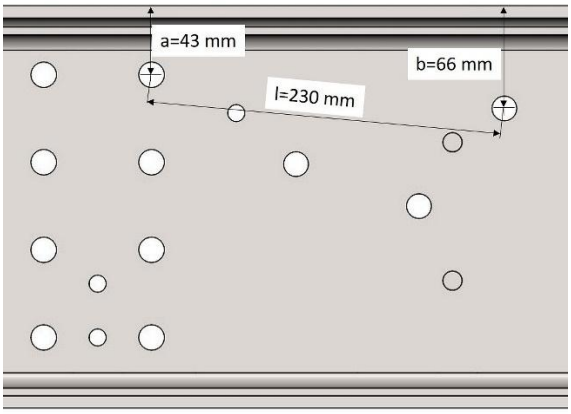


Figure 4. Location of the transducer mounting point.

The average elongation of the upper flange of the longitudinal member over a length corresponding to the base of the strain gauge (for example, 3 mm) gives a value of approx. 4.8 μm. This value is too small to be used to monitor frame stress. Therefore, the role of the transducer base was to concentrate the deformations on a small area measured by the strain gauge sensor, while not exceeding the permissible stresses, taking into account the phenomenon of material fatigue.

The material appropriate for the transducer base should have the following characteristics: fine-grained, homogeneous structure, high strength, low deformation hysteresis as a function of load, good thermal conductivity and low Young's modulus sensitivity to temperature changes [36,37]. Material 1.8159 [38] was selected with the parameters shown in Table 1.

Table 1. Characteristics of the transducer material (1.8159) [38].

Material	Young's modulus [MPa]	Temperature coefficient of Young's modulus $\frac{\Delta E}{\Delta T}\ [\frac{10^{-5}}{K}]$	Thermal expansion coefficient $\alpha\ [\frac{10^{-6}}{K}]$
1.8159	E=2,1x10^5	-26	11

Steel 1.8159 can be heat-treated to achieve the strength parameters shown in Table 2.

Table 2. Steel 1.8159 strength parameters after heat treatment [39].

Re [MPa]	Rm [MPa]	A [%]	Z [%]
~900	1100÷1300	min. 9	min. 40

Taking the above into account and analysing the location of the transducer installation, it was assumed that the mounting space occupied by the transducer should not exceed approximately 50x50x250 mm.

3.2. Transducer base design

Several design assumptions were made with regard to the transducer base element. It was assumed that it should be characterized by relatively high elongation at low stiffness, relatively high deformation concentration in the area measured by the strain gauge sensor, which depends only on elongation and does not depend on other forms of deformation, and stresses not exceeding 30% of the yield strength. Assuming that R_e=900 MPa, the stresses should not exceed σ=270 MPa. The Finite Element Method was chosen to analyze the geometry of successive iterations of the transducer base in order to identify the regions of greatest deformation and the reduced stress values. In addition, the area around the strain gauge installation spots should be protected against mechanical damage, contamination, and water access. Due to existing limitations resulting from the layout of other elements of the other systems at the transducer mounting location, the external dimensions should not exceed

250x50x50 mm. Topological optimization based on the adopted criteria was carried out in four iterations. The first approximation of the shape is shown in Figure 5. The central cylindrical part of the transducer was the planned installation site for the strain gauges. Due to its shape, this space could be relatively easily closed (sealed) by adding covers with seals. However, the resulting stresses at a given increase in the distance between the mounting points (Δl=0,5 mm) reached values that exceeded the yield strength of the material used.

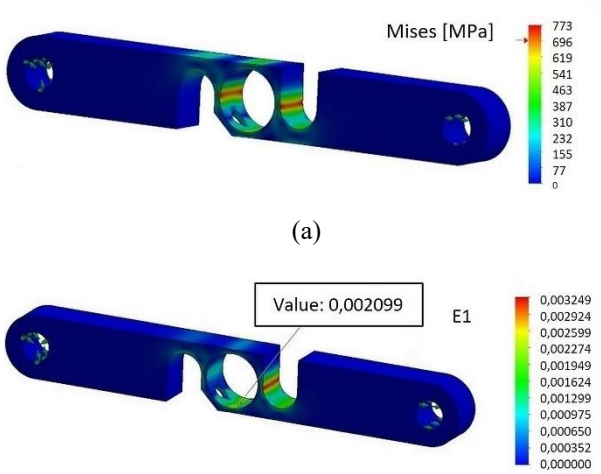


Figure 5. Simulation results of the first iteration of the transducer base in terms of stress (a) and deformation (b) ($\Delta l = 0{,}5$ mm).

The results of the second iteration simulation of the transducer base design are shown in Figure 6. The dimensions of the connectors between the mounting points and the measurement area were changed. This resulted in a favourable but insufficient reduction in stress and an unfavourable reduction in deformation. Therefore, a third iteration was performed, introducing further changes to the transducer base design, which consisted of changing the dimensions of the connectors and reducing the wall thickness of the cylindrical part of the measurement area. The results of the simulation of the stress and strain distribution of the third iteration of the base transducer are shown in Figure 7. A further reduction in stresses below the allowable value was achieved. In terms of strains, a further reduction was achieved, which was considered a significant drawback. After the analysis, changes (fourth iteration) were made that consisted of increasing the diameter of the measuring part of the transducer base, as shown in Figure 8. Simulation tests were performed on the modified version, the results of which are presented in Figures 9 and 10.

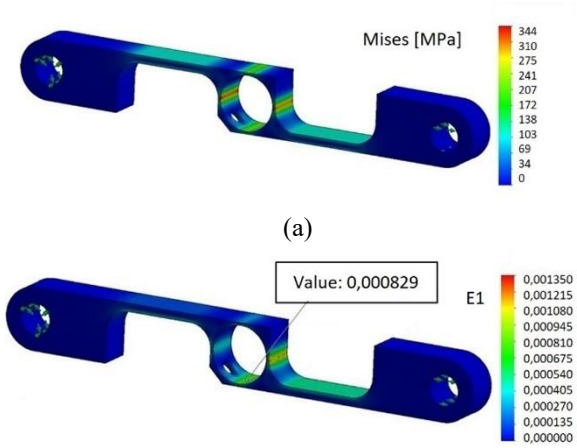


Figure 6. Simulation results of the second iteration of the transducer base in terms of stress (a) and deformation (b) ($\Delta l = 0{,}5$ mm).

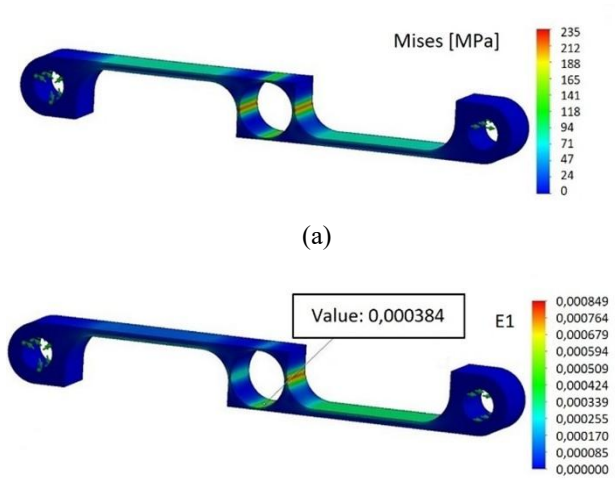


Figure 7. Simulation results of the third iteration of the transducer base in terms of stress (a) and deformation (b) ($\Delta l = 0{,}5$ mm).

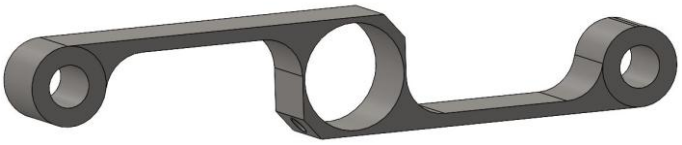


Figure 8. Accepted transducer base design.

FEM simulations of stress and strain distribution were performed for the transducer base geometry established in the fourth iteration, as shown in Figures 9 and 10. The simulation assumed a limited range of changes in the distance between the mounting points of Δl=±0,5 mm.

The maximum stresses did not exceed 259 MPa, which was approximately 29% of R_e=900 MPa.

At the same time, significantly large deformations were obtained in the predicted zone of strain gauge installation, as shown in Figure 10.

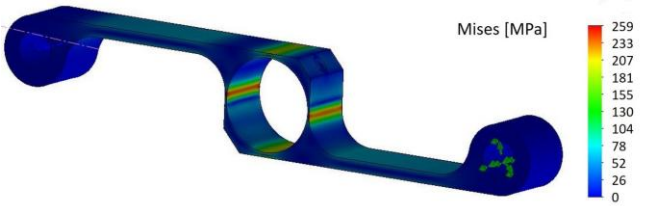


Figure 9. Stress distribution during the extension of the base of the transducer by Δl=+0,5 mm.

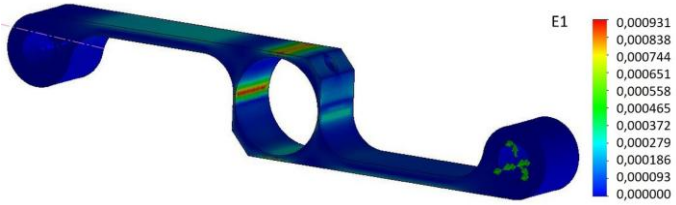


Figure 10. Distribution of principal strains E1 during an extension of the transducer base by $\Delta l = 0{,}5$ mm.

The stress and strain results obtained for the fourth iteration of the transducer base were concluded to meet the preliminary requirements. Data illustrating the quality of the FEM simulation are summarized in the table 3.

Table 3. Set of FEM data.

Details mesh type	solid mesh	Mesh quality	high
Mesher used	blended curvature-based mesh	Total nodes	714630
Jacobian points for high quality mesh	16 points	Total elements	490511
Max. element size	1 mm	Max. aspect ratio AR	25,126
Min. element size	0,3333 mm	Percentage of elements with AR<3	99,9

A mesh sensitivity analysis was performed using the h method (SolidWorks Simulation) to ensure that the convergence of the results was above 97% and that the computation time did not exceed 1 minute.

3.3. Strain gauge sensor arrangement

A strain gauge measuring system consisting of strain gauges ($R = 350\Omega, k = 2{,}1$) connected in a full Wheatstone bridge [36,38] and aligned so that the directions of strain in the transducer base matched the axes of the strain gauges (red arrows in Figure 11). This arrangement provided temperature compensation. The connection diagram of the strain gauges is shown in Figure 11.

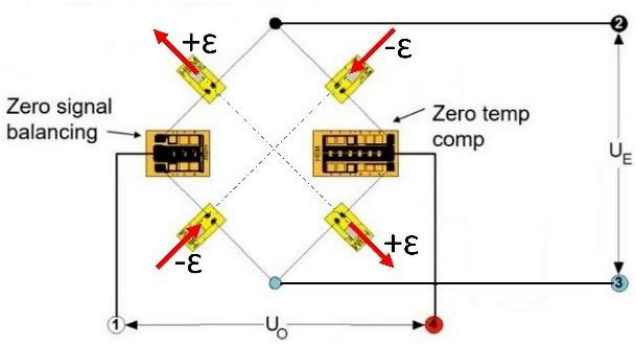


Figure 11. Wiring diagram for strain gauges in a Wheatstone bridge connection.

The measuring section of the transducer with bonded and connected strain gauges is shown in Figure 12.

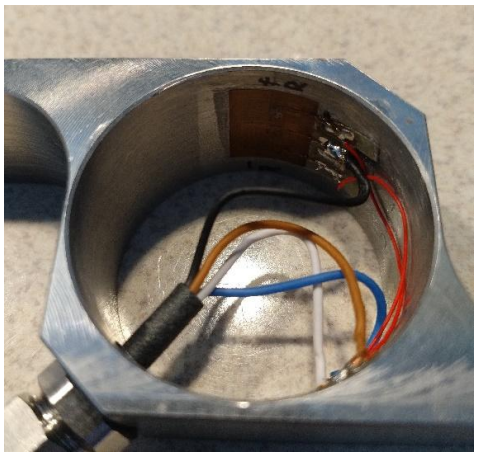


Figure 12. Measurement system in a Wheatstone bridge circuit.

Table 4. Specifications for selected strain gauges 1-XY71-3/350 and adhesive Z70.

1	with soldering points
X	Two measuring grids, measuring grid direction: X-shaped, offset by 90°
Y	Carrier and covering agent: polyimide / Measuring grid foil: constantan
7	Type and position of the connections
1	Material to which the strain gauge temperature response is matched: ferritic steel
3	Measuring grid length in mm
350	Measuring grid resistance in ohms
Z70	Bonding material for experimental stress analysis and transducer, tamp. range: -55°C ÷ +100°C

The location of the strain gauge sensors, as well as their type and dimensions, were determined by the strain field established in FEM simulation tests. These tests revealed a concentration of strain on the area marked in red, which was approximately 4 mm wide (Fig. 10). Consequently, the effective length of the strain gauge sensors was set to l = 3 mm. The strain gauges and the adhesive used for their installation were selected so that the expected ambient temperature range (±50°C) would not exceed

the permissible range specified by the manufacturer. Furthermore, the strain gauge sensors featured self-compensating temperature compensation (self-compensated SG). A summary of the selected strain gauge data for the measurement system is presented in the table 4.

3.4. Scaling the transducer

After completion of the measurement system based on the transducer, it was scaled, i.e., the relationship between the changes in the measured value and the load was determined. General guidelines for scaling can be found in [40]. A view of the measuring stand is shown in Figure 13. The transducer was loaded with weights in increments of 5 kg and then unloaded in increments of 10 kg. The characteristics of the transducer are presented in Table 5 and illustrated in the graph in Figure 14.



Figure 13. The measurement stand for performing transducer scaling.

Table 5. Transducer characteristics.

Load, kg	0,8	5,8	10,8	15,8	20,8	25,8	30,8	35,8	40,8
Strain, μm	58	378	700	1018	1338	1655	1973	2289	2606
Load, kg	40,8		30,8		20,8		10,8		0,8
Strain, μm	2606		1977		1343		703		59
Hysteresis, Δμm	0		4		5		3		1

The linearised strain characteristic of the transducer is described by the equation:

$$\varepsilon = 63{,}7m + 10{,}2 \tag{3}$$

where:

ε – strain, $\mu m/m$,

m – load (mass), kg.

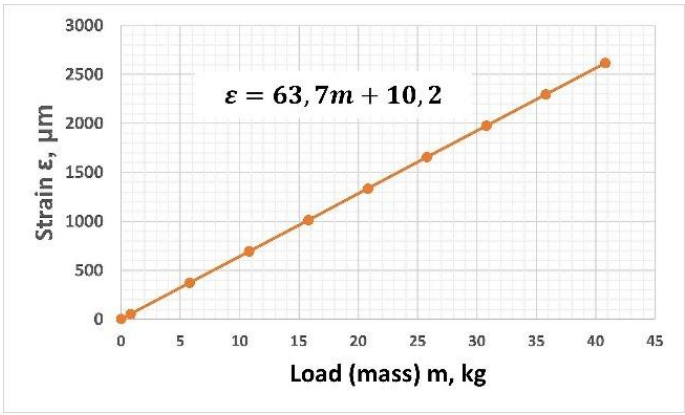


Figure 14. Linearised strain characteristic of the transducer.

3.5. Correction of strain gauge unbalance in a Wheatstone bridge circuit

When installing strain gauges on a prepared transducer base, their initial deformation is forced (to fit the bonding surface), which introduces a certain measurement asymmetry into the measurement circuit of each bridge arm, reflected as a difference in resistance between points 2-4 and 3-4, and 1-2 and 1-3, e.g.:

$$\Delta R = \frac{R_{24}}{R_{34}} \neq 0 \tag{4}$$

To eliminate unbalance, the zeroing of the unloaded system indication should be performed using, for example, an additional resistor in the form of an adhesive compensation strain gauge with a fixed step change in resistance [38], shown in Figure 9, or made of thin wire with the same (or similar) temperature coefficient of resistance as the measuring strain gauges. The additional compensation resistance R_C can be determined by performing the following calculations.

Case 1 – Wheatstone bridge unbalance expressed in mV/V units, e.g.:

$$\frac{U_{14}}{U_{23}} = \frac{1}{4}\frac{\Delta R_T}{R_{SG}} \neq 0 \tag{5}$$

$$\Delta R_T = \alpha \cdot R_O \cdot \Delta T = \alpha_C \cdot R_C \cdot \Delta T \tag{6}$$

After substituting (6) into (5) and transforming, we obtain the following:

$$R_C = 4 \cdot \frac{U_{14}}{U_{23}} \cdot \frac{R_{SG}}{\alpha_C \cdot \Delta T} \tag{7}$$

The required length of the additional resistance wire L_C, the

addition of which will balance the circuit branch, can be determined as follows:

$$R_C = L_C \cdot R_{C0} \tag{8}$$

$$L_C = \frac{4}{R_{C0}} \cdot \frac{U_{14}}{U_{23}} \cdot \frac{R_{SG}}{\alpha_C \cdot \Delta T} \tag{9}$$

where:

ΔR_T – change of resistance caused by a change in temperature, Ω,

α_C – coefficient of change in wire material resistance as a function of temperature, $\frac{\Omega/\Omega}{K}$,

R_C – resistance of a resistor made of thin wire with a fixed cross-section, Ω,

ΔT – ambient temperature range, K,

R_{SG} – resistance of a strain gauge, Ω,

R_{C0} –specific resistance, Ω/m,

L_C – calculated wire length to balance the Wheatstone bridge, m,

Case 2 – Wheatstone bridge unbalance expressed in $\mu m/m$ units, e.g.:

$$\frac{\Delta R_T}{R_{SG}} \neq 0 \tag{10}$$

$$\frac{\Delta R_T}{R_{SG}} = k \cdot \varepsilon \rightarrow \Delta R_T = k \cdot \varepsilon \cdot R_{SG} = \alpha_C \cdot R_C \cdot \Delta T \tag{11}$$

$$R_C = L_C \cdot R_{C0} \tag{12}$$

$$L_C = \frac{k \cdot \varepsilon \cdot R_{SG}}{\alpha_C \cdot R_{C0} \cdot \Delta T} \tag{13}$$

where:

ε –strain, $\mu m/m$,

k – gauge factor.

As can be seen in Figure 12, the transducer would require correction of the initial indication:

$$m = 0 \rightarrow \varepsilon = 10{,}2\,\frac{\mu m}{m} = 10{,}2 \cdot \frac{10^{-6} m}{m} \tag{14}$$

Assuming:

- ambient temperature range: $\Delta T = 100\ K$,
- resistance of a strain gauges: $R_{SG} = 350\ \Omega$,
- gauge factor: $k = 2{,}1$,
- specific resistance of copper wire with a diameter of 0,04 mm: $R_{Cu} = 0{,}014\ \Omega/m$,
- coefficient of change in wire material resistance as a function of temperature: $\alpha_{Cu} = 0{,}004\ \frac{\Omega/\Omega}{K}$,

the required length of wire can be determined:

$$L_C = \frac{k \cdot \varepsilon \cdot R_{SG}}{\alpha_{Cu} \cdot R_{C0} \cdot \Delta T} = \frac{2{,}1 \cdot 10{,}2 \cdot 10^{-6} \cdot 350}{0{,}004 \cdot 0{,}014 \cdot 100} \cong 1{,}3\ mm \tag{15}$$

One of the Wheatstone bridge arms 1-2 and 1-3 with lower resistance should be made longer by $L_C = 1{,}3\ mm$ (difficult to implement in practice).

3.6. Preliminary transducer tests

The made transducer shown in Figure 15 was installed on a Jelcz universal chassis without body and underwent very preliminary tests.



Figure 15. Prototype of a longitudinal member deflection transducer for a load-bearing structure.

The range of possible loads on the frame longitudinal member during tests was limited due to the lack of a body. The tests were limited to lifting the wheels of the second axle to a height such that the wheels of the first axle hung freely without contacting the ground, as shown in Figure 16.

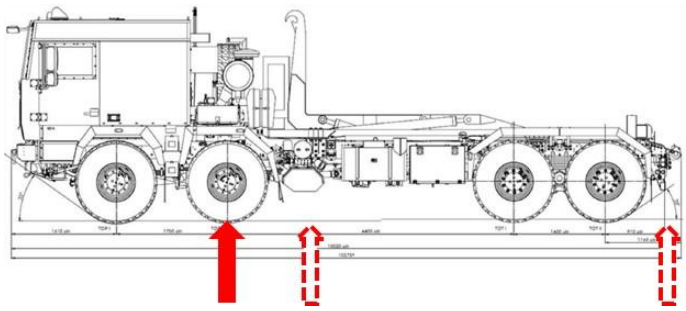


Figure 16. Vehicle lift point (the contour arrows indicate the ultimate vehicle lift points after the installation of the bodies).

During initial tests, the transducer indicated a strain value of 577 ± 5 µm, which is several times higher than the value that could be obtained by applying strain gauges directly to the frame member. This high value indicates the transducer's high sensitivity.

3.7. Overload registration system

The main task of the system was to acquire and process measurement data in order to identify events when the set threshold value associated with the permissible stress of the

load-bearing structure was exceeded [35]. After analysing the available devices, a PLC controller [41] was selected, the basic data of which are presented in Table 6.

Table 6. Short description of the PLC controller [41].

Cortex A8/1 GHz /512MB RAM - 4GB RAM expansion - 32 GB – (SD card)	Operating system: LINUX	Communication: CANopen, TCP,ETHERNET, MQTT, RS-232, RS-485,



Figure 17. PLC controller with expansion cards for analogue voltage signals.

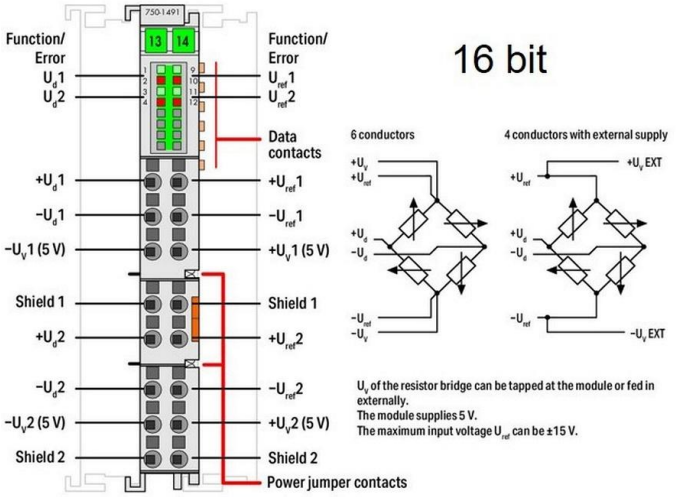


Figure 18. Diagram of strain gauge connections in a 4-wire or 6-wire Wheatstone bridge circuit to analog I/O card [41].

The accepted device was configured to work with a wide range of devices that extend functionality, including input cards for voltage signals. The constructed recorder is shown in Figure 17. It had 10 input channels for operating strain gauges connected in a 4-wire or 6-wire Wheatstone bridge configuration, with the possibility of expanding to 32 measurement channels. The strain gauge connection diagram is shown in Figure 18. Software was written to operate the controller, which produced a vector of information about the structure: CH,YYYY,MM,DD, HH,MM,SS,V, i.e.: CH – measurement channel, YYYY – year, MM – month, DD – day, HH – hour, MM – minute – SS – second, V – measured value. Event recording was made conditional, i.e. only threshold exceedances were recorded, which could be edited. Values below the input threshold were measured, but not recorded.

Detailed information on the processing of measured signals by the analog I/O card can be found in the documentation provided by the manufacturer [42]. The selected data are presented in the table 7.

Table 7. The chosen data of analog I/O card 750-1491.

Signal voltage U_D	from $\pm 15mV$ to $\pm 360mV$	Resolution [bit]	16
Signal voltage U_{ref}	5V	Measurement error (25°C)	U_D:$\pm 30\mu V$, U_{ref}: $\pm 0{,}05\%$

At this stage of the research, no analyses were conducted regarding measurement signal filtering and noise suppression.

4. Discussion

The design of the transducer base met the initial dimensional requirements and allowed the system to be installed on the vehicle in the available mounting space at the post-production stage, which did not affect the vehicle assembly process. Taking into account the existing mounting holes in the side members during the transducer design stage and adopting a modular design for the entire system allows it to be installed on vehicles already in service. The design of the transducer, including the shape of the measuring space, allows for its hermetic sealing, and thus does not limit the vehicle's performance parameters, e.g., fording. However, the miniaturization of the transducer base at the point of deformation measurement significantly limits the possibility of using ready-made compensation strain gauges for zero compensation. Hence, there was a need to perform such compensation in an alternative way. However, the calculated change in the length of the connection in the relevant arms of the Wheatstone bridge (L_c=1,3 mm) posed a certain objective difficulty in constructing a measuring system with the required accuracy and, as a result, obtaining a zero indication. However, this inaccuracy should not be of great practical significance, as the controller software provides for the possibility of entering a threshold value that can take into account the initial imbalance of the measuring system.

The preliminary results of the experimental tests were

limited to a very short series of measurements taken under conditions that were different from the ultimate operating conditions of the vehicle. For organisational reasons, it was not possible to perform full tests in a vehicle preloaded with specialised equipment. However, the experimental tests reflected the basic load on the frame side members caused by raising the body to its working position. After installing the specialised equipment on a container platform equipped with extendable supports, the vehicle would be lifted at the points marked with contour arrows in Figure 16. It can be expected that the resulting deformation of the frame side members would be greater. Nevertheless, the recorded value of 577 μm seems to be sufficient to track changes in the loads on the longitudinal members of the frame during lifting the entire body.

The measurement system implemented in the transducer, which uses self-compensating strain gauges connected in a full Wheatstone bridge configuration, along with zero-point compensation, minimizes measurement errors (e.g., temperature drift). Furthermore, it should be noted that the measurement was performed while the vehicle body was being lifted, which limited the duration of the measurement. It should also be noted that a measurement range exceeding 2600 μm protects the transducer from being damaged by, for example, an overload of the load-bearing structure. Furthermore, simply adding the transducer base to the vehicle's side member does not, in practice, affect the stiffness of the entire load-bearing structure. The force required to cause a 0.5 mm elongation of the transducer base (twice the allowable elongation limited by the strength of the side member) was approximately 400 N, which can be considered a negligible value.

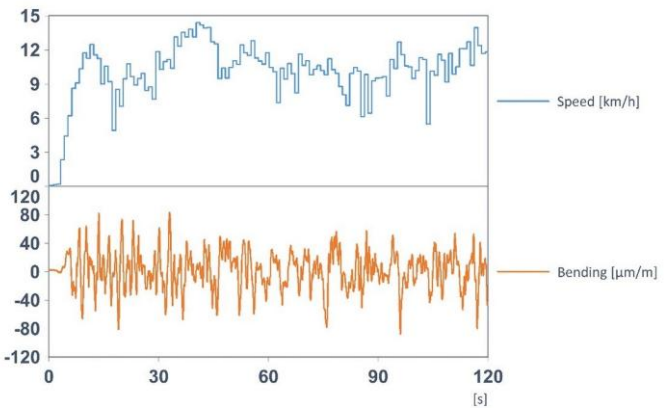


Figure 19. The range of recorded strains on the section of off-road.

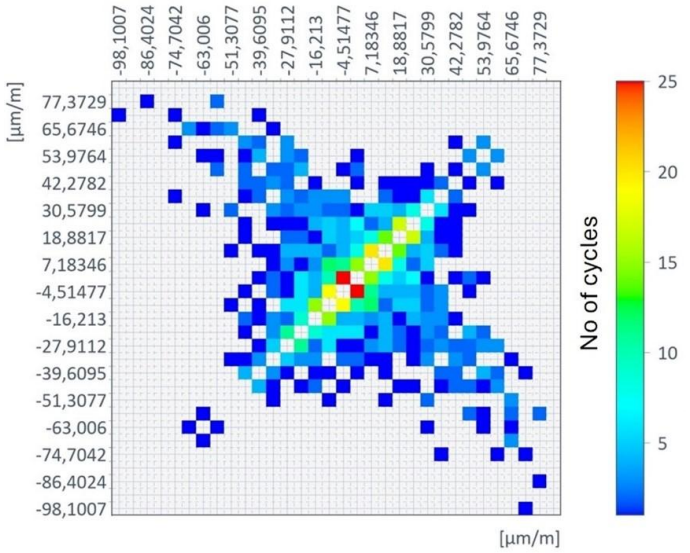


Figure 20. No of cycles recorded on off-road.

A significant limitation of the presented solution is the fact that the transducer cannot be placed where the greatest deformations occur. Furthermore, at this stage of the research, the transducer did not record deformations caused by torsion of the longitudinal member, which can occur when the structure is lifted non-parallel. This limitation can be overcome by installing a set of two transducers on two longitudinal members. The ability to independently measure tension and torsion is a complex issue, because in this case constrained torsion of transducer base occurs, and it would be necessary not only to place a strain gauge sensor measurement system to measure torsion but also to separate the torsion signal component from the total tension signal. This problem has not yet been solved.

The encouraging results obtained from the transducer tests are motivation to explore new research directions and areas of application for the transducer. One such ongoing research project is the search for a solution to track operational loads that would take into account a vehicle's load history, the driver's driving style and factors related to the type of road. Such data would be useful for identifying vehicles (within a group of the same vehicle type) with the highest remaining useful life. In other words, it would be possible to identify which vehicle is the one with the smallest overall deterioration and is the most reliable. Preliminary limited tests were conducted on a section of an off-road track, recording the signal corresponding to the bending of the frame side member. The load history and vehicle speed are shown in Figure 19. The recorded data was filtered using the Rainflow algorithm [43], obtaining a set of

deformation amplitude values in conjunction with the number of cycles, as shown in Figure 20. The ability to obtain load distributions (deformations and/or stresses) in combination with the number of cycles provides a basis for developing a numerical index that accounts for the influence of traffic conditions and the driver's driving style.

5. Conclusion

The proof-of-concept (PoC) design of the overload monitoring system for the load-bearing structure of a high-mobility wheeled vehicle met the initial requirements. In the context of vehicle health and usage monitoring systems (HUMS), the solution presented is limited and restricted to significant, although exceptional cases of operational loads. The designed transducer can be subjected to an elongation of up to 0.5 mm, which results in a measurement signal exceeding 2600 μm at a tension/compression force of only about 400 N. The dimensions of the transducer base's mounting space have been limited to approximately 250x50x50 mm. The measurement system, consisting of self-compensating strain gauges connected in a Wheatstone bridge, ensures a stable measurement signal. The possibility of waterproofing the measurement space does not limit the range of applications for the vehicle itself. These features of the solution not only allow the initial objectives to be achieved but also open up new application possibilities.

References

1. ASTM E1926:2021, *Standard Practice for Computing International Roughness Index of Roads from Longitudinal Profile Measurements*. https://store.astm.org/e1926-08r21.html; 2026 [accessed 22.04.2026].
2. ISO 8608:2016, *Mechanical vibration — Road Surface profiles — Reporting of measured data*. https://www.iso.org/standard/71202.html; 2026 [accessed 22.04.2026].
3. NO23-A502-1:2010, *Military technology - Research of military mechanical vehicles - Part 1: Introduction, requirements and recommendations*. https://wcnjik.wp.mil.pl/; 2026 [accessed 17.04.2026].
4. Grašič L, Lerher T, Rosi B. Evaluating costs of vehicle use in military logistics. *Tehnicki vjesnik - Technical Gazette* 2016; 23(6):1679-1686. https://doi.org/ 10.17559/TV-20150522141708.
5. PDNO-23-A503:2017, *Military vehicles – Reliability tests*. https://wcnjik.wp.mil.pl/; 2026 [accessed 17.04.2026].
6. *Wsparcie i zabezpieczenie techniczne Sił Zbrojnych RP. Zasady funkcjonowania*, DD-4.22(A), Warszawa; 2017.
7. *Instrukcja zarządzania eksploatacją sprzętu wojskowego w Siłach Zbrojnych RP. Zasady ogólne*, DD-4.22.13(A), Warszawa; 2018.
8. *Condition-Based Maintenance Plus Guidebook*, Office of the Deputy Assistant Secretary of Defense for Materiel Readiness, Office of the Under Secretary of Defense for Acquisition and Sustainment, Washington, DC. https://www.cto.mil/wp-content/uploads/2024/08/Eng-Def-Sys-Change1-July2024.pdf; 2024 [accessed 22.04.2026].
9. IEC 60300-3-11:2009, *Dependability management - Part 3-11: Application guide - Reliability centred maintenance*. https://webstore.iec.ch/en/publication/1296; 2026 [accessed 15.04.2026].
10. Ochando F.J, Cantero A, Guerrero J.I, Leon C. Data Acquisition for Condition Monitoring in Tactical Vehicles: On-Board Computer Development, *Sensors* 2023; 23: 5645. https://doi.org/10.3390/s23125645.
11. Anonymous. Prognostics and health management for the JSF program. *Sound and Vibration* 2004; 38(5): 8.
12. Rabeno E, Bounds M. Condition Based Maintenance of military ground vehicles. In: *IEEE Aerospace conference*, Big Sky, MT, USA; 2009. pp. 1-6. https://doi.org/10.1109/AERO.2009.4839683; 2026 [accessed 11.04.2026].
13. U.S.Army Aberdeen Test Center. https://www.atecciviliancareers.com/organizations/atc; 2026 [accessed 22.04.2026].
14. GPMS Begins Machine Condition Monitoring Demonstration with AM General and US Army HUMVEE Vehicles. https://www.gpms-vt.com/news/machine-condition-monitoring-with-am-general-and-us-army-humvee-vehicles; 2026 [accessed 17.04.2026].
15. Scheina C. Abrams demonstration proves concept for enterprise-level system health monitoring. https://www.army.mil/article/238848/abrams_demonstration_proves_concept_for_enterprise_level_system_health_monitoring; 2026 [accessed 17.04.2026].
16. Bundeswehr Technical Center for Land-Based Vehicle Systems, Engineer and General Field Equipment (WTD). https://www.bundeswehr.de/en/organization/equipment/structure/wtd-41; 2026 [accessed 17.04.2026].
17. Direction generale de l'armement. https://www.defense.gouv.fr/dga/dga-techniques-terrestres; 2026 [accessed 17.04.2026].

18. A success for the use of HUMS for Land equipment support: Tactical Evaluation Vérité. https://www.arquus-defense.com; 2026 [accessed 16.04.2026].
19. UTAC Millbrook proving Ground. https://www.army-guide.com/eng/firm3456.html; 2026 [accessed 17.04.2026].
20. PIRANHA 5 Armoured Wheeled Vehicle. https://www.army-technology.com; 2026 [accessed 17.04.2026].
21. Panther Command and Liaison Vehicle (CLV). https://www.army-technology.com; 2026 [accessed 17.04.2026].
22. Wojskowy Instytut Techniki Pancernej i Samochodowej. https://witpis.pl/dzialalnosc/pion-badan/lbp/; 2026 [accessed 17.04.2026].
23. MIL-STD 810H:2022, *Environmental engineering considerations and laboratory tests*. https://assist.dla.mil/online/login/welcome.cfm; [accessed 22.04.2026].
24. Heine R, Barker D. Simplified terrain identification and component fatigue damage estimation model for use in a health and usage monitoring system, *Microelectronics Reliability* 2007; 47: 1882-1888. https://doi.org/10.1016/j.microrel.2007.02.017.
25. Siłuch D, Droździel P, Pukalskas S, Evaluating vehicle repair duration in relation to driving styles. *Eksploatacja i Niezawodność – Maintenance and Reliability* 2025; 27(2): 195746. https://doi.org/10.17531/ein/195746.
26. Kosobudzki M. The use of acceleration signal in modeling proces of loading an element of underframe of high mobility wheeled vehicle. *Eksploatacja i Niezawodnosc – Maintenance and Reliability* 2014; 16(4): 595-599.
27. Kosobudzki M, Stańco M. Problems in assessing the durability of a selected vehicle component based on the accelerated proving ground test. *Eksploatacja i Niezawodnosc – Maintenance and Reliability* 2019; 21(4): 592-598. http://dx.doi.org/10.17531/ein.2019.4.8.
28. Stańco M, Kaszuba M, Herbik I. Identification of Factors Leading to Damage of Semi-Elliptical Leaf Springs. *Materials* 2025; 18(23): 5426. https://doi.org/10.3390/ma18235426.
29. Stańco M, Kowalczyk M. Analysis of Experimental Results Regarding the Selection of Spring Elements in the Front Suspension of a Four-Axle Truck. *Materials* 2022; 15(4): 1539. https://doi.org/10.3390/ma15041539.
30. Stafanow D. The Impact of Transfer Case Parameters on the Tractive Efficiency of Heavy Off-Road Vehicles. *Sustainability* 2025; 17(19): 8586. https://doi.org/10.3390/su17198586.
31. Kilby T.S, Rabeno E, Harvey J. Enabling Condition Based Maintenance with Health Usage Monitoring Systems. In: *AIAC14 Fourteenth Australian International Aerospace Congress Seventh DSTO International Conference on Health & Usage Monitoring (HUMS 2011)*, Australia; 2011. https://apps.dtic.mil/sti/citations/ADA387225; [accessed 22.04.2026].
32. Ludovici D, Bray M, Wickramanayake V. Health and usage monitoring proof of concept study using army land vehicles. *8th DSTO International Conference on Health and Usage Monitoring (HUMS 2013)*, Australia; 2013. https://researchcentre.army.gov.au/; [accessed 10.04.2026].
33. MSPO 2024: WZŁ-1 w programie Wisła i Narew. https://defence24.pl/mspo/mspo-2024-wzl-1-w-programie-wisla-i-narew; 2024 [accessed 17.04.2026].
34. Podwozie Jelcz P882D.43. https://jelcz.com.pl/oferta/nieopancerzone-8-x-8; 2026 [accessed 17.04.2026].
35. Iluk A, Andruszko J. Obliczenia wytrzymałościowe ustroju nośnego pojazdu Jelcz M43 AŁC-T z uwzględnieniem jazd w warunkach terenowych. Sprawozdanie nr 37/2024 (raport niejawny). Wydział Mechaniczny PWr; 2024.
36. Styburski W. *Przetworniki tensometryczne. Konstrukcja, projektowanie, użytkowanie*. Wydawnictwa Naukowo-Techniczne WNT, Warszawa: 1971.
37. Hoffmann K, *An introduction to measurements using strain gauges*. Hottinger Baldwin Messtechnik GmbH, Darmstadt: 1989.
38. *The route to measurement transducers. A guide to the use of the HBM K series foil strain gages and accessories*. HBM GmbH, Darmstad: 2008.
39. EN 10083-3:2008, *Steels for quenching and tempering – Part 3: technical delivery conditions for alloy steels*. https://sklep.pkn.pl/pn-en-10083-3-2008p.html,access; 2026 [accessed 20.04.2026].
40. ISO 376:2011, *Metallic materials – calibration of force-proving instruments used for the verification of uniaxial testing machines*. https://www.iso.org/obp/ui/es/#iso:std:iso:376:ed-4:v1:en; 2026 [accessed 26.04.2026].
41. Sterownik PLC WAGO 750-8412. https://www.wago.com/pl/; 2026 [accessed 17.04.2026].
42. *WAGO Automation Technologies*, ed. 2026-1, WAGO GmbH & Co. KG. https://www.wago.com/pl/systemy-i-o/moduł-wejść-analogowych-2-kanałowy/p/750-1491#downloads; 2026 [accessed 29.06.2026].

43. ASTM E1049-85:2005, *Standard practices for cycle counting in fatigue analysis*. https://store.astm.org/e1049-85r05.html; 2026 [accessed 26.04.2026].